Calculation of Separation Bubbles Using a Partially Parabolized Navier-Stokes Procedure

D. H. Choi* and D. J. Kang†
Korea Advanced Institute of Science and Technology, Seoul, Korea

A partially parabolized Navier-Stokes solution procedure for the transitional separation bubble has been developed. By coupling with the far-field potential-flow solution, the calculation domain can be kept relatively small to minimize the computation time. Using the eddy-viscosity turbulence model of Baldwin and Lomax, it is shown that the procedure is capable of capturing the details of the separation bubble. The results are in excellent agreement with experimental data and exhibit a marked improvement over those of existing interactive boundary-layer procedures for the cases examined.

Introduction

THE transitional separation bubble developed on an airfoil surface has been of great research interest for many years due to its direct bearing on the stall characteristics. The bubble is characterized by the separation of the laminar boundary layer, followed by the transition and subsequent reattachment as a turbulent boundary layer. The knowledge and prediction of this process pose a practical importance as the performance of many engineering devices, such as aircraft and turbomachinery, are closely related to the phenomenon.

To understand the features associated with the bubble and, possibly, to come up with some simple criteria for bubble breakdowns, there have been numerous experimental studies since the late 1940s.[1-6] The theoretical approach to the problem has also been explored and progress has been made. In an effort to get a quick solution for the bubble growth and bursting, Horton[7] and Roberts[8] developed semi-empirical criteria that could be used in an integral scheme. Crimi and Reeves[9] proposed a transition model in their integral formulation for the leading-edge bubble analysis. However, for an accurate and detailed solution, one needs to resort to a more elaborate scheme based on the finite-difference method. The most widely used method of this type to date is the interactive boundary-layer (IBL) procedure.[10-12]

The method lies basically within the framework of the thin boundary-layer approximation: it is assumed that the viscous layer is thin and the surface curvature is small in relation to the bubble size. This justifies the use of boundary-layer equations and also allows the bubble effect on the external velocity to be accounted for by the equivalent source distribution over the surface, i.e., through the Hilbert integral. Briley and McDonald's[13] procedure also falls in this category, although they used a stream function/vorticity form of Navier-Stokes equations.

The IBL procedure in general can be effective when the flow meets the basic assumption. However, the breakdown of the approximation is evident where the surface curvature is relatively large: the bubble can no longer be considered small and, consequently, the Hilbert integral does not adequately simulate the displacement effect. Most of the leading-edge separation bubbles are likely to fall in this category. In a recent study by the present authors,[14] it is shown that the curvature terms play a significant role even for the bubble developed near midchord.

One alternative to overcome this difficulty is the use of Navier-Stokes equations. Since the equations are valid for both viscous and inviscid regions, the need for an interaction mechanism between the viscous and inviscid flows can be avoided. The purpose of this paper is to present a new procedure, based on partially parabolized Navier-Stokes (PPNS) equations with a simple eddy-viscosity turbulence model. The calculation domain is chosen carefully to achieve both accuracy and efficiency. The method is very straightforward in principle. However, it differs from the existing methods in two major respects: 1) the viscous/inviscid interaction is accounted for by the use of PPNS equations, and 2) all the higher order curvature terms are retained in these equations. It will be demonstrated, through a series of calculations, that this new procedure successfully resolves the aforementioned shortcomings associated with the IBL procedure. Also discussed in the paper is the transition model. Using the result of present calculations, the transition criteria of Crimi and Reeves[9] and Kwon and Pletcher[12] are evaluated. An attempt is then made to devise a model, which is similar to that of Kwon and Pletcher.

Analysis Procedure

Governing Equations

Starting from the Reynolds-averaged Navier-Stokes equations in the general orthogonal curvilinear coordinate system given in Nash and Patel,[15] we obtain the two-dimensional partially parabolized equations by dropping the streamwise diffusion terms. These two momentum equations and the continuity equation are written in a body-fitted coordinate system, with ξ being parallel to the surface and η normal to it:

$$\frac{U}{h_1}\frac{\partial U}{\partial \xi}+\frac{V}{h_2}\frac{\partial U}{\partial \eta}+(K_{12}U-K_{21}V)V+\frac{1}{h_1}\frac{\partial}{\partial \xi}(p+\overline{u^2})+\frac{1}{h_2}\frac{\partial}{\partial \eta}(\overline{uv})+2K_{12}\overline{uv}+K_{21}(\overline{u^2}-\overline{v^2})-\frac{1}{Re}[L_1(U)+L_2(V)]=0 \tag{1}$$

$$\frac{U}{h_1}\frac{\partial V}{\partial \xi}+\frac{V}{h_2}\frac{\partial V}{\partial \eta}+(K_{21}V-K_{12}U)U+\frac{1}{h_1}\frac{\partial}{\partial \xi}(\overline{uv})+\frac{1}{h_2}\frac{\partial}{\partial \eta}(p+\overline{v^2})+2K_{21}\overline{uv}+K_{12}(\overline{v^2}-\overline{u^2})-\frac{1}{Re}[L_1(V)-L_2(U)]=0 \tag{2}$$

Received March 12, 1990; revision received Aug. 27, 1990; accepted for publication Sept. 24, 1990.

*Professor, Department of Mechanical Engineering. Member AIAA.
†Graduate Student, Department of Mechanical Engineering.

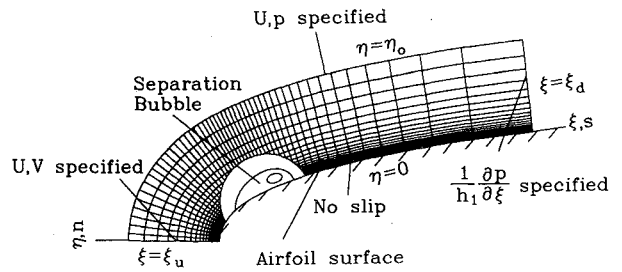

Fig. 1 Schematic of the computation domain and boundary conditions.

$$\frac{1}{h_1}\frac{\partial U}{\partial \xi}+\frac{1}{h_2}\frac{\partial V}{\partial \eta}+K_{21}U+K_{12}V=0 \tag{3}$$

where

$$L_1=\frac{1}{h_2^2}\frac{\partial^2}{\partial \eta^2}+(K_{21}-K_{11})\frac{\partial}{h_1\partial \xi}+(K_{12}-K_{22})\frac{\partial}{h_2\partial \eta}-K_{21}^2-K_{12}^2$$

$$L_2=2\left(K_{12}\frac{\partial}{h_1\partial \xi}-K_{21}\frac{\partial}{h_2\partial \eta}\right)+\frac{1}{h_1}\frac{\partial K_{12}}{\partial \xi}-\frac{1}{h_2}\frac{\partial K_{21}}{\partial \eta}$$

$$K_{12}=\frac{1}{h_1h_2}\frac{\partial h_1}{\partial \eta}, \text{ etc.}$$

and where (U,V) and (u,v) are, respectively, the mean and fluctuating velocity components in the (ξ,η) direction, p the pressure, Re the Reynolds number, and h and K the metric coefficients and curvature parameters. It should be noted that these equations are exact other than the neglected diffusion terms and have been made dimensionless by the freestream velocity U_∞ and the airfoil chord c.

Turbulence Model

A closure relationship of the simplest type, a zero-equation model, is advantageous as the entire flowfield, where both laminar and turbulent regimes are present, can be described by a small number of equations, Eqs. (1-3). Among many variations, the algebraic eddy-viscosity model of Baldwin-Lomax[16] is adopted due to its convenient way of determining the length scale. The length scale is determined from the distribution of vorticity, and therefore the need for locating the outer edge of a shear layer can be avoided. It is appropriate to note here that the model, being an equilibrium turbulence model, may suffer some degradation in its performance in the regions of flow separation and reattachment. However, the fact that there is no widely accepted turbulence model for such regions, together with the convenience stated previously, prompted the present choice.

Once the eddy-viscosity ν_t is determined, the Reynolds stresses in Eqs. (1) and (2) are then related to the mean rate of strain through the following Boussinesq hypothesis:

$$-\overline{u^2}=\nu_t\left(\frac{2}{h_1}\frac{\partial U}{\partial \xi}+2K_{12}V\right)-\frac{2}{3}k$$

$$-\overline{v^2}=\nu_t\left(\frac{2}{h_2}\frac{\partial V}{\partial \eta}+2K_{21}U\right)-\frac{2}{3}k$$

$$-\overline{uv}=\nu_t\left(\frac{1}{h_1}\frac{\partial V}{\partial \xi}+\frac{1}{h_2}\frac{\partial U}{\partial \eta}-K_{12}U-K_{21}V\right) \tag{4}$$

where k denotes the turbulent kinetic energy. Since k is not solved explicitly in the present model, it is provided from the widely used empirical relationship $k=-\overline{uv}/0.3$.

Boundary Conditions

Equations (1-3) together with the closure relationships in Eq. (4) are solved in the domain that encompasses the separation bubble shown in Fig. 1. Since the equations are parabolic for the velocity components U and V and elliptic for pressure p, the following conditions are prescribed along each boundary:

Upstream:

$$\xi=\xi_u \qquad U,V \text{ specified}$$

Downstream:

$$\xi=\xi_d \qquad \frac{\partial p}{h_1\partial \xi} \text{ specified}$$

Outer:

$$\eta=\eta_0 \qquad U,p \text{ specified}$$

Wall:

$$\eta=0 \qquad U=V=0 \tag{5}$$

The values of V along the outer boundary ($\eta=\eta_0$) and p along the wall ($\eta=0$) are determined implicitly by the governing equations and thus need not be prescribed.

The outer boundary is placed sufficiently far away from the surface so that the viscous effects, including that of the bubble, become negligible; the conditions of potential flow are assumed to apply. At the same time, the boundary needs to be close to the surface to achieve the computational efficiency. About 20 times the maximum boundary-layer thickness in the bubble region was found to be adequate in this study. The assumption may, however, break down when a massive separation occurs on the airfoil. This will alter the flow severely near the leading edge and the attached flow solution will not give the real conditions at the present boundary. In such cases, one may resort to other inviscid schemes that take the separation effect into account in the calculation.[17] For the present study, a low-order (linear) panel method based on the surface potential distribution, in which each panel is represented by a straight segment and the potential on each panel is assumed constant, is employed to obtain the outer-boundary conditions. These conditions may be improved by updating the potential-flow solution using the equivalent surface transpiration. No attempt has been made, however, to do this as the effects are believed to be secondary and the coding becomes more complex.

To construct the velocity profiles along $\xi=\xi_u$, a separate boundary-layer calculation from the stagnation point is performed. This will provide the profiles inside the boundary layer, and a smooth fairing of these profiles to the potential-velocity distributions of the outer layer completes the inlet condition. It should be pointed out that the velocity components U and V can be of comparable magnitude in the outer layer around the leading edge.

The Neumann condition for pressure along the downstream boundary $\xi=\xi_d$ is again obtained from the potential-flow solution. It was observed that, although the variation in pressure across the section is not negligible, the derivative in ξ direction remains fairly constant. Therefore, unlike at the upstream boundary, the distinction between the inner and outer sections has not been made.

Transition

Flow changes from laminar to turbulent gradually through the intermittent region. It is simulated by the intermittency factor γ, which is given by

$$\gamma=1-\exp[-0.025(s-s_{tr})^2/\delta_s^{*2}] \tag{6}$$

as was used in Refs. 9 and 12. Here, s is the arc length, δ^* the displacement thickness, and the subscripts s and tr denote the points of separation and transition, respectively.

The prediction of the onset of transition remains the most difficult aspect in the analysis. Since the burgeoning of flow instability depends on so many parameters, such as the profile

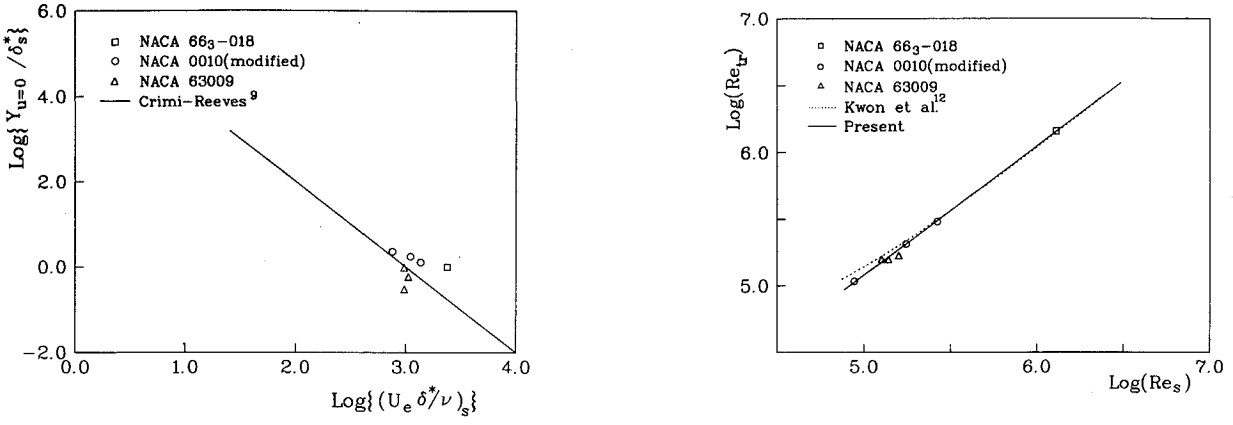

a) Crimi-Reeves model b) Kwon-Pletcher model

Fig. 2 Comparison of the present results with existing transition criteria.

shape, pressure gradient, freestream turbulence level, etc., determining the transition point rigorously yet practically seems years away. Recent work by Cebeci[18,19] may represent a step in such direction. An alternative way that has been in use is empirically established transition models. Among these, the following two models of Crimi and Reeves[9] (CR) and Kwon and Pletcher[12] (KP) have been examined closely for the present study. Crimi and Reeves used an integral boundary-layer analysis to correlate the bubble height at transition to the displacement thickness at separation:

$$\frac{y\,|_{U=0}}{\delta^*_s} = \frac{10^6}{(U_e\delta^*/\nu)^2_s} \tag{7}$$

Kwon and Pletcher, on the other hand, examined a wide range of experimental data, i.e., pressure distributions, and proposed the following correlation:

$$Re_{\rm tr} = 1.0607\ Re_s + 33185 \tag{8}$$

where Re is based on the distance along the surface from the stagnation point.

To assess the validity of these models, calculations, the procedure of which will be described in the following section, were made for various cases. Instead of applying Eqs. (7) and (8) directly, the transition location was varied continuously for each case to find one that best reproduced the experimental data. It is recognized that the transition point so obtained is, to a certain extent, turbulence-model dependent and may vary slightly for a different turbulence model. Assuming this to be the correct transition location, the parameters of CR and KP models were then obtained from the result and are compared with Eqs. (7) and (8) in Fig. 2 denoted by the symbols □, ○, and △. Although the present results lie in the vicinity of the CR correlation in Eq. (7), as seen in Fig. 2a, the substantial scatter hardly makes the model reliable. The discrepancy is believed to be the result of an integral approach used in the CR analysis. A similar comparison is made against the KP model and shows a good agreement in Fig. 2b. Since the KP model is based on the experimental correlation, the good agreement also indicates that the present results are compatible with the experimental data. The slight deviation noted in the low-Reynolds-number region may be attributed to the uncertainty in the data, i.e., the points of stagnation, separation, and transition.

Instead of using Eq. (8), we fit a straight line through the points by using the least squares approximation and obtain

$$Re_{\rm tr} = 1.76\ Re_s^{0.967} \tag{9}$$

The model is by no means complete because of its limited basis. However, judging from its agreement with Eq. (8), it is expected to perform reasonably well for a wider range of flows.

Solution Procedure

The finite-difference algorithm of Galpin et al.[20] is modified to treat the turbulent flow and used for the present calculation. Using a staggered grid system, Eqs. (1-3) with the expression for the Reynolds stresses in Eq. (4) are first discretized. Here, the central differencing is used except for the streamwise convective derivatives that are discretized by upwind differencing. The resulting difference equations can be arranged in the following form:

Continuity:

$$U_{i,j} = f_1(V_{i,j+1},\ V_{i,j}) \tag{10}$$

ξ momentum:

$$p_{i,j} = f_2(U_{i,j-1},\ U_{i,j},\ U_{i,j+1}) \tag{11}$$

η momentum:

$$V_{i,j} = f_3(V_{i,j-1},\ V_{i,j},\ V_{i,j+1},\ p_{i,j-1},\ p_{i,j}) \tag{12}$$

where the variables in the coefficients of nonlinear terms or in the source terms assumed the most recent values and are not listed as arguments.

Equations (10) and (11) are then substituted into Eq. (12) and the pentadiagonal equation for V results:

$$C_{NN}V_{i,j+2} + C_N V_{i,j+1} + C_P V_{i,j} + C_S V_{i,j-1} + C_{SS}V_{i,j-2} = B \tag{13}$$

where the coefficients C and the source term B are functions of U, V, and p at the previous iteration step. Marching downstream, Eq. (13) is solved for V at each ξ station by using the pentadiagonal matrix solution algorithm described in Galpin et al.[20] The quantities U and p are then evaluated from Eqs. (10) and (11). Two local iterations are performed to resolve nonlinearity.

After one complete sweep, the pressure is updated to enhance the upstream pressure propagation and thus expedite the convergence. This is done by requiring the ξ-momentum equation to be satisfied, on the average, along the constant ξ line. The correction on the i line, assuming that $p_{i+1,j}$ have already been updated, is given by

$$\delta p_i = \frac{\sum_{\text{all } j} C_j\,(p_{i+1,j} - p_{i,j}) + \cdots}{\sum_{\text{all } j} C_j} \tag{14}$$

where the numerator for each j represents the discretized ξ-momentum equation at node (i,j) and becomes zero upon convergence.

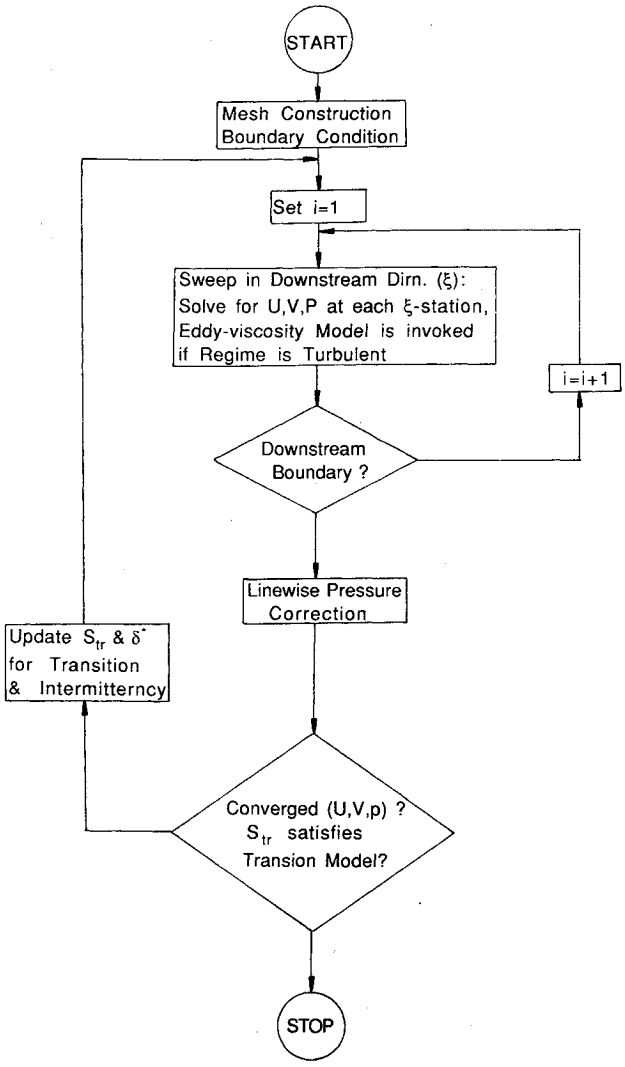

Fig. 3 Solution procedure.

The process is repeated until the pressure and velocities converge. The maximum variation in two successive iterations of 10^{-3} is found to be adequate and used as a criterion for convergence. With a 100×80 grid, about 200 iterations are needed for a typical bubble calculation. The transition point is updated after each iteration. A gradual change in transition location is essential in obtaining stable convergence behavior.[14] The overall procedure is shown in Fig. 3. It should be noted that, unlike in Ref. 20, the sweep in η direction is not performed in the present procedure.

Results and Discussion

A few test calculations have been made with the procedure described in the previous section. Among various experimental cases, only the ones that do not exhibit the massive separation were selected for this purpose. The reason for this is to obtain the potential-flow solution, which is used as boundary conditions, without much uncertainty. A 100×80 nonuniform grid is fitted over each domain with the nodes concentrated near the wall and inside the bubble.

Calculations are made with both forced (prescribed) and model [Eq. (9)] transitions. The results for three different NACA airfoil sections—modified 0010, 63-009, and 66_3-018—at various incidences and Reynolds numbers are compared with the data. Comparisons are also made with some IBL results.

For the modified NACA 0010 section, calculations are performed at 8-deg incidence for three different chord Reynolds numbers, namely 2, 4, and 6×10^6. The domains for these calculations are $0.027 < s/c < 0.263$ and $n/c < 0.017$, 0.013, and 0.013, respectively. Here s is the distance measured along the surface from the stagnation point; n is the distance normal to the surface, and each value corresponds to about 20 times the maximum boundary-layer thickness in the region as was mentioned earlier. The pressure for all three cases are shown in Fig. 4. The points of separation, transition, and reattachment are denoted as S, T, and R, respectively, in the figure. These are in good agreement with the experimental data of Gault.[3] Results with the forced and model transitions are nearly identical, as is expected from Fig. 2b. Calculation has also been performed for $Re = 2 \times 10^6$ with a 120×100 grid to check the grid dependency of the solution. The results are in close agreement with each other, as shown in Fig. 4, and confirm that the 100×80 grid is fine enough to resolve the flowfield.

To examine the performance more closely, the results for $Re = 2 \times 10^6$ are compared with those of Vatsa and Carter[11] in Fig. 5. The data of Vatsa and Carter are taken graphically from Ref. 11 and, therefore, are subject to some uncertainty. The surface pressure distribution of the undisturbed potential flow is also shown for reference.

Vatsa and Carter used an IBL technique to get their solution. Here, the pressure on which the boundary-layer calculation was based, called reference pressure, was obtained from an independent viscous airfoil analysis; the pressure peak of this solution matches well with that of the experimental data. Although the results show the similar characteristics of the experiment, the pressure distribution ahead of the bubble is not well predicted. Calculation fails to reproduce the nearly

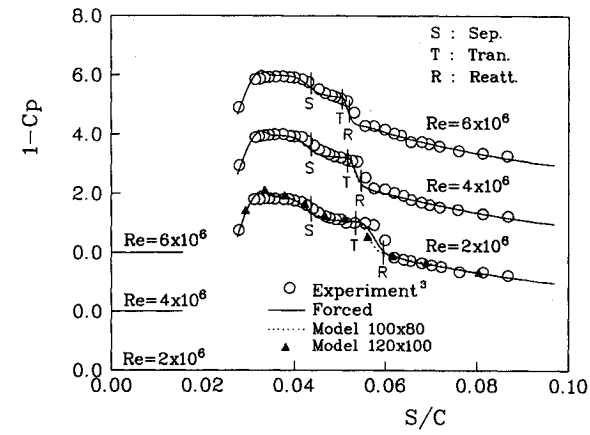

Fig. 4 Pressure distribution on the modified NACA 0010 section at $\alpha = 8$ deg for various Reynolds numbers.

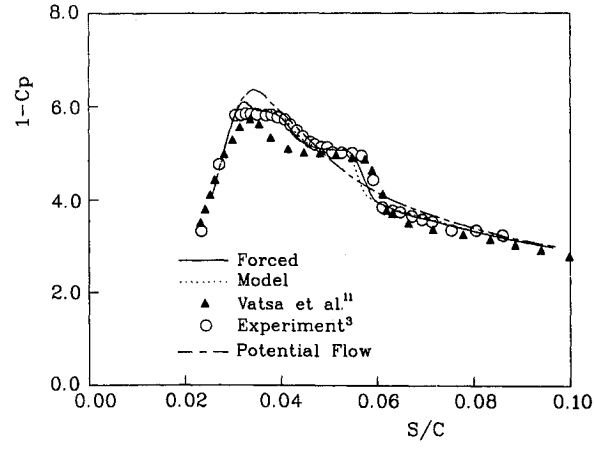

Fig. 5 Comparison of pressure distributions in the vicinity of the bubble; modified NACA 0010 section, $\alpha = 8$ deg and $Re = 2 \times 10^6$.

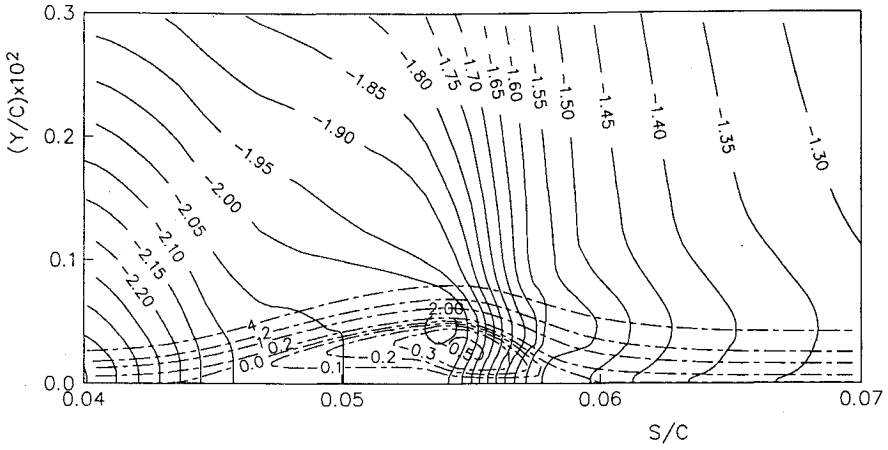

Fig. 6 Streamlines and isobaric lines near the bubble for the modified NACA 0010 section at $\alpha = 8$ deg and $Re = 2 \times 10^6$.

flat peak pressure. Calculated pressure is generally lower in this region. It also gives a lower pressure in the downstream region. The latter discrepancy suggests that the reference pressure may not be accurate.

On the other hand, the present solution exhibits a near perfect agreement with the data. The improvement over the IBL solution is remarkable and can be directly attributed to the implicit interaction mechanism of the Navier-Stokes approach coupled with the curvature terms in the equations. Sufficiently far away from the bubble, the pressure recovers the attached potential-flow value and the excellent agreement in this region implies that the pressure variation across the domain is well captured by the present scheme. It is clear that the Hilbert-integral approach for the interaction is deficient in treating flows developed along such highly curved surfaces, even when the bubble is only 2% of the chord long. The good agreement, together with Vatsa and Carter's result, leads us to believe that the local interaction with the bubble, not a global mechanism, is solely responsible for the drop in the pressure peak from its potential-flow value. Pressure deviation from the potential flow indicates that the bubble, which extends from $s/c \approx 0.043$ to 0.062 as is shown in Figs. 6 and 7, influences the pressure distribution well outside of its region: from $s/c \approx 0.03$ to 0.08.

The streamlines and isobaric contours near the bubble for the same case are shown in Fig. 6. The pressure varies very little in the laminar region of the bubble. As the flow becomes turbulent, the pressure recovers rapidly through the transient to the turbulent portion of the bubble. A peculiar local maximum of the pressure, which is observed at the height of the bubble where the transition occurs, has probably been caused by the rapid change in the streamline curvature and is believed to be of numerical nature. It also needs to be pointed out that the flow inside the bubble forms a single vortex as is evidenced in the figure. This is in contrast with the earlier result of Davis and Carter[21] where two counter-rotating vortices were observed.

Figure 7 shows the displacement-thickness and the shear-stress distributions for all three cases. The locations of separation, transition, and reattachment are indicated in the figure. The growth rate of the displacement thickness δ^* suddenly becomes large at a short distance upstream of the separation point and is maintained until the transition process begins. Then δ^* drops rather sharply before the flow redevelops as the turbulent boundary layer well downstream of the reattachment. The shear-stress distribution C_f, exhibits the size of the bubble for each case, and C_f remains fairly constant in the laminar portion of the bubble. It then drops rapidly after the point of transition in the process of adjustment to become turbulent flow. The kinks in the C_f curves near $s/c = 0.035$

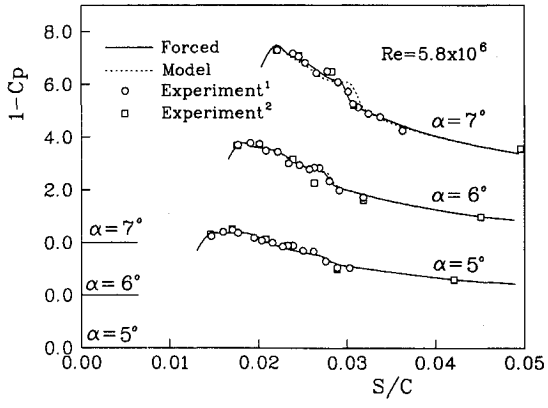

Fig. 8 Pressure distributions on the NACA 63-009 section for $Re = 5.8 \times 10^6$ at various incidences.

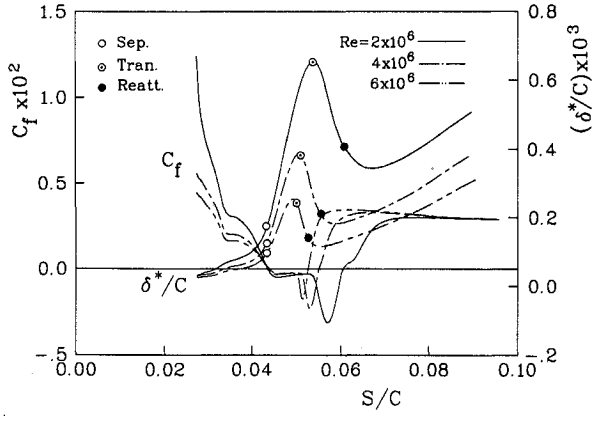

Fig. 7 Shear-stress and displacement-thickness distributions for the modified NACA 0010 section at $\alpha = 8$ deg and $Re = 2 \times 10^6$.

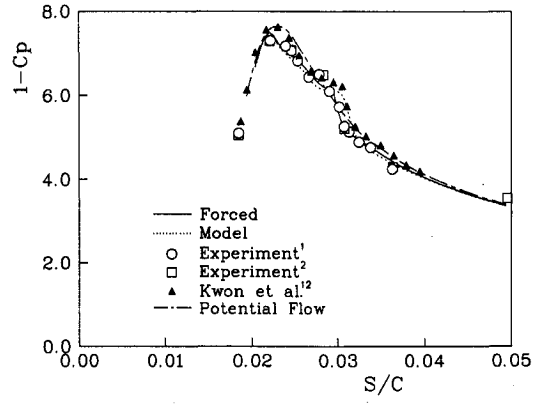

Fig. 9 Comparison of pressure distributions in the vicinity of the bubble for the NACA 63-009 section at $\alpha = 7$ deg and $Re = 5.8 \times 10^6$.

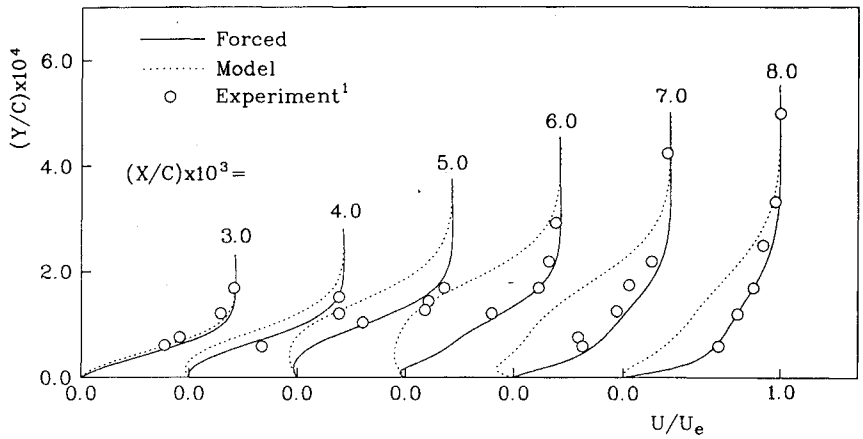

Fig. 10 Velocity profiles at various locations on the NACA 63-009 section for $\alpha = 7$ deg and $Re = 5.8 \times 10^6$.

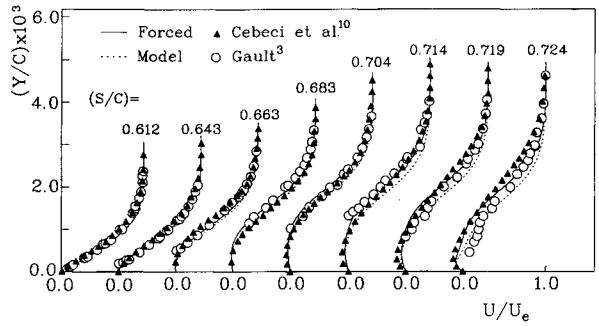

Fig. 11 Comparison of velocity profiles on the NACA 66_3-018 section for $\alpha = 0$ deg and $Re = 2 \times 10^6$.

are due to the curvature variation in the airfoil surface and are not of any significance.

The results for a NACA 63-009 section for $Re = 5.8 \times 10^6$ at $\alpha = 5$, 6, and 7 deg are presented in Figs. 8–10. The pressure distributions are again compared with the experimental data of Gault[1] and McCullough and Gault[2] in Fig. 8. The same level of agreement as for the previous cases is observed. As can be expected from the scatter in Fig. 2b, the result with the transition model, Eq. (9), for $\alpha = 7$ deg agrees with the data least favorably. Figure 9 compares the pressure distribution for $\alpha = 7$ deg with the IBL result of Kwon and Pletcher.[12] It is confirmed that the presence of the bubble is felt well outside of the bubble, and the IBL method is less successful in bringing down the suction peak to the desired level.

Integral parameters, C_f, δ^*, streamlines, and pressure contours all behave similarly to those of previous cases and therefore are not presented here. Figure 10 depicts the velocity profiles at various locations for $\alpha = 7$ deg. A good agreement with the data can be seen for the calculation with prescribed transition. The transition model, Eq. (9), gives much thicker profiles as it predicts a later transition. It is somewhat disappointing to see such a large discrepancy in velocity result from a seemingly small shift in the transition location. Pressure, on the other hand, is much less sensitive to this change as we see in Fig. 8. The highly sensitive response of the velocity seems to suggest that the profile shapes should be taken into consideration in developing a transition model.

Finally, among the results of NACA $66_3 - 018$ airfoil section at $\alpha = 0$ deg and $Re = 2 \times 10^6$, only the velocity profiles are compared in Fig. 11. The calculation has been carried out in the domain $0.33 < s/c < 0.85$ and $n/c < 0.04$. This case is different from the previous two examples in that the bubble is developed near the midchord and thus the curvature effect is expected to be less. In view of the fact that the velocity is more sensitive than other quantities, the results for both forced and model transitions can be considered to be in good agreement with the experimental data.[3] Also compared in the figure is the IBL solution of Cebeci and Schimke.[10] It should be noted, however, that the transition point in their calculation is not the same as the present one. Unlike the earlier cases where IBL methods fared less satisfactorily, the IBL results are in close agreement with the others. This may indicate that the IBL method with the Hilbert-integral-type pressure correction performs better when the surface curvature is small.

Concluding Remarks

It has been shown that the PPNS solution procedure described herein is capable of predicting the complex flow features of the transitional separation bubble. The PPNS equations provide a natural interaction mechanism of viscous and inviscid flows; retention of the higher order curvature terms helps capture details of the flow around a highly curved surface. Optimal placement of the outer boundary, by incorporating the potential-flow solution, enables the method to achieve both efficiency and accuracy. The results presented here are in much better agreement with the experimental data than those of existing IBL procedures, especially in the leading-edge region. Given the correct transition location, the present scheme accurately simulates separation, reattachment, and, above all, the substantial reduction in the pressure peak.

Calculations with both prescribed and model transitions give comparable results in general. However, the velocity appears to be very sensitive to the change in the transition location and a further improvement on the transition model is desired. It requires a thorough examination of major parameters to develop a widely applicable model. The present procedure could play a useful role in conducting such a study since it can supplement the flow data that is obtained from experiments.

Acknowledgments

This research was sponsored by the Korea Engineering and Science Foundation. The authors are grateful to V. C. Patel for reviewing the paper and for the helpful discussions.

References

[1]Gault, D. E., "Boundary Layer and Stalling Characteristics of the NACA 63-009 Airfoil Section," NACA TN 1894, June 1949.

[2]McCullough, G. B., and Gault, D. E., "Example of Three Representative Types of Airfoil-Section Stall at Low Speed," NACA TN 2502, Sept. 1951.

[3]Gault, D. E., "An Experimental Investigation of Region of Separated Laminar Flow," NACA TN 3505, Sept. 1955.

[4]Weibust, E., Bertelrud, A., and Ridder, S. O., "Experimental Investigation of Laminar Separation Bubbles and Comparison with Theory," *Journal of Aircraft*, Vol. 24, No. 5, 1987, pp. 291–297.

[5]O'Meara, M. M., and Mueller, T. J., "Laminar Separation Bubble Characteristics on an Airfoil at Low Reynolds Numbers," *AIAA*

Journal, Vol. 25, No. 8, 1987, pp. 1033–1041.

[6]Tani, I., "Low-Speed Flows Involving Bubble Separation," *Progress in Aeronautic Science,* Vol. 5, 1964, pp. 70–103.

[7]Horton, H. P., "A Semi-Empirical Theory for the Growth and Bursting of Laminar Separation Bubbles," *Aeronautical Research Council,* CP 1073, 1969.

[8]Roberts, W. B., "Calculation of Laminar Separation Bubbles and Their Effect on Airfoil Performance," *AIAA Journal,* Vol. 18, No. 1, 1980, pp. 25–31.

[9] Crimi, P., and Reeves, B., "Analysis of Leading-Edge Separation Bubbles on Airfoils," *AIAA Journal,* Vol. 14, No. 11, 1976, pp. 1548–1555.

[10]Cebeci, T., and Schimke, S. M., "The Calculation of Separation Bubbles in Interactive Turbulent Boundary Layers," *Journal of Fluid Mechanics,* Vol. 131, 1983, pp. 305–317.

[11]Vatsa, V. N., and Carter, J. E., "Analysis of Airfoil Leading-Edge Separation Bubbles," *AIAA Journal,* Vol. 22, No. 12, 1984, pp. 1697–1704.

[12]Kwon, O. K., and Pletcher, R. H., "Prediction of Subsonic Separation Bubble on Airfoils by Viscous-Inviscid Interaction," *Proceedings of a Symposium on Numerical and Physical Aspects of Aerodynamic Flows II,* edited by T. Cebeci, Springer Verlag, New York, 1984, pp. 163–171.

[13]Briley, W. R., and McDonald, H., "Numerical Prediction of Incompressible Separation Bubbles," *Journal of Fluid Mechanics,* Vol. 69, 1975, pp. 631–656.

[14]Choi, D. H., and Kang, D. J., "Surface Curvature Effect on the Calculation of Separation Bubble," *AIAA Journal,* Vol. 27, No. 9, 1989, pp. 1288–1290.

[15]Nash, J. F., and Patel, V. C., "Three-Dimensional Turbulent Boundary Layers," *SBC Technical Books,* 1972.

[16]Mehta, U., Chang, K. C., and Cebeci, T., "A Comparison of Interactive Boundary-Layer and Thin-Layer Navier-Stokes Procedures," *Proceedings of a Symposium on Numerical and Physical Aspects of Aerodynamic Flows III,* edited by T. Cebeci, Springer Verlag, New York, 1986, pp. 198–215.

[17]Dvorak, F. A., and Choi, D. H., "Separation Model for Two-Dimensional Airfoils in Transonic Flow," *AIAA Journal,* Vol. 22, No. 8, 1984, pp. 1064–1070.

[18]Cebeci, T., "Numerical Instability in the Calculation of Laminar Separation Bubbles and Their Implications," *AIAA Journal,* Vol. 27, No. 5, 1989, pp. 656–658.

[19]Cebeci, T., "Essential Ingredients of a Method for Low Reynolds Number Airfoils," *AIAA Journal,* Vol. 27, No. 12, 1989, pp. 1680–1688.

[20]Galpin, P. F., Van Doormaal, J. P., and Raithby, G. D., "Solution of the Incompressible Mass and Momentum Equations by Application of a Coupled Equation Line Solver," *International Journal of Numerical Methods in Fluids,* Vol. 5, 1985, pp. 615–625.

[21]Davis, R. L., and Carter, J. E., "Counter-rotating Streamline Pattern in a Transitional Separation Bubble," *AIAA Journal,* Vol. 24, No. 5, 1986, pp. 850, 851.